,

PAPER

Augmented Stabilized Formulations with Fictitious Boundary Methods

R. Ranjan[a*], Y. Feng[b], A. Chronopoulos[c]

[a] *Senior Computational Modeler, Astronautics Corporation of America, Madison*
[b] *Professor, Department of Mechanical Engineering, University of Texas San Antonio*
[c] *Professor, Department of Computer Science, University of Texas San Antonio*;

(*v3.0 released May 2009*)

Augmentation of the SUPS formulation was introduced earlier and successfully applied to solving incompressible Navier- Stokes equations for both two dimensional and three dimensional problems. Fictitious boundary methods (FBM) is a new methodology that aid the study of flow descriptions around solid obstacles on fixed Cartesian product grids that do not require body confirming meshes. FBM has been applied to lower order finite element and spectral/*hp* least squares techniques. We test the augmented stabilized finite element formulation introduced earlier, (ASUPS) to the fictitious boundary context and use it to solve incompressible flow problems. Utilizing the advantages of fictitious boundary methods we present solutions to flow around an array of two dimensional and three dimensional problems. In two dimensional flow computations we solve flow past a circular and elliptical shaped cylinders. For the ellipse shaped obstacles in a Newtonian flow field we examine the effects of varying boundary conditions and aspect ratios on the flow metrics. Finally we extend the procedures to solving two ellipse and two circular shaped obstacles facing the free stream. In three dimensional computations we examine incompressible flow around a three dimensional ellipse shaped obstacle at Reynolds number Re-200.

Keywords: Fictitious Boundary Methods; spectral/*hp* methods; Augmented stabilized finite element (ASUPS); Incompressible Flow; Stabilized Formulations

1. Introduction

Flow around complex geometries is a fundamental problem in Computational Fluid Dynamics with applications in studying particulate flows, flow past various different shaped obstacles, sedimentation, debris flows etc. (1). Studying such flows invariably requires an intricate meshing in the vicinity of the solid domain where the boundary layers develop. These flow problems require both the region in the near vicinity of the solid domain and the liquid domain to be meshed and consequent flow features resolved. Such meshing constraints can take substantial development time while solving problems. An alternative to body fitted meshing techniques is the usage of a fixed Cartesian product grid. There are two competing approaches that have been proposed in this category for solving solid-liquid flows. The first is the arbitrary lagrangian-eulerian (ALE) method where both the fluid and the particle equations of motion are incorporated into a single coupled variational equation. An attractive alternative to the ALE method is the Fictitious Boundary Method (FBM). This procedure falls under the general category of 'fixed grid' approaches where the need to frequently remesh the domain is obviated. In this paper we present two different approaches to examining the solid-fluid coupled flow problem with the FBM formulation. The first constructs a modified functional which incorporates the velocity profile as a penalty term that is consequently minimized. The second method utilizes a simplified approach with the specification of the velocity

*Corresponding author. Email: ranrakesh@gmail.com

components directly on the governing nodes of the solid domain. Both the solid and the fluid domains are meshed as a single Cartesian product grid in both the approaches examined. The solid domain is implicitly defined on the underlying fluid domains.

Extensive research in computational fluid dynamics in the last few decades has resulted in proposal of different methodologies for solving incompressible flow Navier-Stokes equations. Different numerical schemes namely finite volume, finite difference, and finite element methods have been developed. In computational fluid dynamics (CFD) applications the predominant techniques that are still favored are finite volume procedures. Finite volume techniques have gained popularity because the formulation is conservative, and it provides a physical basis to governing physical laws. While the finite volume methods provide flexibility with determining solutions to partial differential equations with a combination of Taylor series expansions and appropriate upwinding techniques there is restricted applicability of the method for unstructured meshes and non uniform meshes. Finite element procedures (FEM) on the other hand provide a more rigorous mathematical framework for the solution of partial differential equations of interest. In finite element literature different methodologies have been proposed for solving incompressible Navier-Stokes equations. The methods that have gained popularity are based on Penalty finite element methods (2), Least Squares type approaches (3; 4; 5), and Stabilized Finite element methodologies (6; 7; 8). Least squares finite element (LSFEM) methods suffer from extensive loss of mass for many problems (e.g. forward facing step, flow through contraction regions) (4; 5). Penalty finite element methods on the other hand suffer from severely ill-conditioned matrix systems which are not amenable for solutions with iterative solvers for large scale problems (2; 9). These limitations prohibit the usage of either Penalty finite element or least squares FEM for solutions of large scale problems.

Stabilization methods for solving advection-dominated problems were introduced by Hughes and Brook (8; 10) and Brooks et al. (6; 7). The optimal upwinding schemes provide nodally exact solutions to advection diffusion problems in one dimension (7). Generalizations to multi-dimensions were also outlined. The streamline upwind Petrov Galerkin finite element method added extra terms to the under-diffused Galerkin finite element formulation, which greatly improved the conditioning of the resulting stiffness matrix. Stabilized finite element methods provide a variational setting for the Navier-Stokes equations and further provide a viable alternative for solving incompressible flow problems in primitive variables. The stabilized finite element method adds flow stabilizing terms to the weak form Galerkin finite element formulation and ameliorates the conditioning issues associated with the Galerkin finite element procedure. Stabilized formulations result in two competing formulations, Galerkin Least Squares procedures (GLS) and the Streamline Upwind Petrov Galerkin (SUPG) and Pressure Stabilized Petrov Galerkin finite element procedures (PSPG). Stabilized finite element methodology with the same specification of Streamline Upwind Petrov Galerkin (SUPG) and Pressure Stabilized Petrov Galerkin (PSPG) stabilization parameter has been named the SUPS formulation for solving incompressible flow (11). This formulation has been extended with an iterative regularization of the incompressibility constraint by (12). The resulting formulation was named the Augmented SUPS (ASUPS) formulation. The ASUPS formulation introduced was utilized for solving an array of benchmark CFD problems. It was demonstrated that the formulation provides improved non-linear convergence behavior compared to the SUPS formulation. In this paper we utilize the formulation of (12). The GLS formulation can be reduced to the SUPS formulation on neglecting the viscous terms. The ASUPS provides a consistent variational setting for solving incompressible Navier-Stokes equations which demonstrates superior non-linear convergence compared to the SUPS formulation. Advantages of both the Penalty method and the stabilized finite element technology are availed in this formulation. Some of the advantages of the ASUPS formulation are as follows;

- It circumvents the need for artificial mass matrix enhancement with the predictor corrector step while solving incompressible flow problems. The true mass matrix is utilized for solving all problems.
- It allows the usage of standard monolithic solvers in conjugation with inexact newton krylov

methods for solving problems.

- Non linear convergence is achieved with the Navier- Stokes in their natural form. This is attributed to an adequate addressing of the velocity-pressure coupling as opposed to a total loss of stability of the discrete form with SUPG formulations.
- Allows the use of alpha family of approximation for stepping the equations in time in a space time decoupled framework.
- More scales in the problem are resolved than are possible with an artificially enhanced mass matrix in effect accessing a larger bandwidth of fine scale problem.

In this paper we test the ASUPS formulation for relative performance with Fictitious Boundary Methods. We utilize two different approaches for approximating the geometry of the obstacle in the flow field. A variational setting for the approximation of the solid body is described. A second approach that forces the velocity components to be constrained to specified values is further examined. Both methods utilized for FBM computations are outlined in detail in this paper and a series of numerical examples are presented to serve as validation benchmarks. We utilize spectral/*hp* methods for solving problems as they allow immense flexibility on coarse macro meshes for solving problems (13; 14; 15; 16). Procedures for solving both Euler-Bernoulli beam theories and Timoshenko beam theory within the *hpk* framework of non uniform rational b-spline methods have been presented in a recent publication of (17). The paper is organized as follows. In Section II we present the governing equations of a stationary solid and fluid domain respectively. The formulations used for solving the governing equations are presented in Section III. We follow with a series of benchmark problems for studying the effectiveness of the methods presented, in Section IV. Finally we draw conclusions from the demonstrated procedures in Section V.

2. Governing Equations

Let us denote the computational domain as a union of the fluid domain Ω_f and the i^{th} particle domain denoted by Ω_i. We assume the domain contains m particles. The total domain comprising of the fluid and the solid particles is thus denoted by $\Omega_T = \Omega_f \cup \Sigma_{i=1}^{m} \Omega_i$. Let us consider the flow of a Newtonian fluid with density ρ, and viscosity μ in Ω_f. Let $t \in [0, T]$ be the temporal domain, where N is the number of space dimensions. Let Γ denote the boundary of Ω_f. The equations of fluid motion that describe the unsteady Navier-Stokes governing incompressible flows are provided by

$$\frac{\partial \mathbf{u}}{\partial t} + \mathbf{u} \cdot \nabla \mathbf{u} = -\nabla p + \frac{1}{Re} \nabla^2 \mathbf{u} + \mathbf{f} \text{ on } \Omega_f \ \forall \ t \ \in [0, T] \tag{1}$$

$$\nabla \cdot \mathbf{u} = 0, \text{ on } \Omega_f \ \forall \ t \ \in [0, T] \tag{2}$$

where, $\mathbf{u}$, $\mathbf{f}$, and p are the velocity, body force, and pressure respectively. Re denotes the Reynolds number, $\nu = \frac{\mu}{\rho}$ is the kinematic viscosity of the fluid, p is the pressure and $\mathbf{u}$ is the fluid velocity. The part of the boundary at which the velocity is assumed to be specified is denoted by Γ_g:

$$\mathbf{u} = \mathbf{g} \text{ on } \Gamma_g \ \forall t \in \ [0, T] \tag{3}$$

The completes the equations for fluid motion. The governing equations of solid motion utilized in the FDM are based on Newton's laws of motion (18). We are concerned with only the angular motion with constant angular velocities and constant translational velocity. For a presentation of the full set of coupled equations we refer to Turek and coauthors (1). The velocity of the solid domain and the fluid domain are made to confirm based on a no-slip velocity at the boundaries of

the solid domain. The velocity of the solid domain comprised of the particle $i \in \Omega_i$ is provided as

$$\mathbf{U}(\mathbf{x}) = \mathbf{U}_i + \omega_i \times (\mathbf{X} - \mathbf{X_i}) \tag{4}$$

Here, $\mathbf{U}_i$ is the translational velocity of the center of the particle Ω_i. The angular velocity of the center of the particle i is ω_i. The Newton-Euler equations of motion governing the motion of the i^{th} particle require the hydrodynamic integration of the forces and torques acting on each particle. These are obtained respectively as

$$\mathbf{F}_i = -\int_{\partial\Omega_i} \sigma \cdot \mathbf{n} d\Gamma_i \tag{5}$$

and

$$T_i = -\int_{\partial\Omega_i} (\mathbf{X} - \mathbf{X}_i) \times \sigma \cdot \mathbf{n} d\Gamma_i \tag{6}$$

To aid the hydrodynamic integral evaluations of the force and torques we introduce a phase indicator function which distinguishes between the solid and the fluid domain. Let us define the function α_i as:

$$\alpha_i(\mathbf{X}) = \begin{cases} 1 \text{ for } \mathbf{X} \in \Omega_i \\ 0 \text{ for } \mathbf{X} \in \Omega_T \setminus \Omega_i \end{cases} \tag{7}$$

With the help of the indicator function we can obtain simplified expressions of the forces and torques on each particle. The outward normal to the i^{th} particle boundary is provided by

$$\mathbf{n}_i = -\nabla \alpha_i \tag{8}$$

The introduction of the function allows the line integrals around the interface of the particle to be replaced with the volume integrals around a layer of cells nearing the interface. The expression for the drag is obtained

$$\mathbf{F}_i = -\int_{\partial\Omega_i} \sigma \cdot \mathbf{n}_i d\Gamma_i = \int_{\Omega_T} \sigma \nabla \alpha_i d\Omega_i \tag{9}$$

The component form of the drag force (F_{Di})and the lift force (F_{Li}) on obstacle i can be obtained as (in two dimensions):

$$F_{Di} = -\int_{\Omega_T} \left[\mu \left(\frac{\partial u}{\partial x}\frac{\partial \alpha}{\partial x} + \frac{\partial u}{\partial y}\frac{\partial \alpha}{\partial y} \right) - p\frac{\partial \alpha}{\partial x} \right] d\Omega_i \tag{10}$$

and

$$F_{Li} = -\int_{\Omega_T} \left[\mu \left(\frac{\partial v}{\partial x}\frac{\partial \alpha}{\partial x} + \frac{\partial v}{\partial y}\frac{\partial \alpha}{\partial y} \right) - p\frac{\partial \alpha}{\partial y} \right] d\Omega_i \tag{11}$$

The above equations complete the equations needed for a description of two-phase flows for which the FDM method has primarily been devised. The solid motion is governed by the Newton-Euler equations of motion and the fluid motion is described with an iteratively regularized incompressibility in conjunction with the SUPS formulation. The finite element formulation resulting from the relaxation of the incompressibility constraint has been named as the Augmented SUPS (ASUPS)

formulation for incompressible flow computations. The paper by (12) provides the details on the stability analysis of the formulation and provides results for some standard benchmark problems in incompressible flow computations. We extend the ASUPS formulation to the FBM context.

The finite element formulation of the above equations is the next step in the formulation. The standard SUPS formulation for incompressible flow starts with the incompressibility and the momentum equations and develops the finite element formulation directly from these equations. Augmented stabilized finite element formulation takes a different approach to the solution of the above equations. The incompressibility equation is relaxed with an iterative penalization of the constraint. The solutions of the incompressibility constraint is approached in an iterative fashion with increasing regularization steps. Iterative regularization of the incompressibility constraint has been found to improve the convergence of the SUPS formulation. The relaxation of the incompressibility constraint is provided by the following equations.

$$\frac{\partial \mathbf{u}}{\partial t} + \mathbf{u} \cdot \nabla \mathbf{u} = -\nabla p + \frac{1}{Re} \nabla^2 \mathbf{u} + \mathbf{f} \text{ on } \Omega_f \ \forall \ t \ \in [0, T] \tag{12}$$

$$\nabla \cdot \mathbf{u} = -\epsilon (p^k - p^{k-1}), \text{ on } \Omega_f \ \forall \ t \ \in [0, T] \tag{13}$$

The following section describes the formulation and some implementation details utilized for solving problems in this paper.

3. Finite Element Formulation

Let us consider the finite element formulation for the Fictitious Boundary Method. Two different finite element formulations for the FBM method are presented. The first method solves the FBM problem with a direct specification of the velocity components to the specified values. Thus we resort to the unmodified ASUPS formulation for incompressible flow. The whole computational domain is subdivided into the fluid domain Ω_f and the particle domain Ω_i. The extensional velocity from the solid domain to the fluid domain (1) connects the velocities in both the fluid and the solid by virtue of the no slip boundary condition. We consider a high order spectral/hp implementation of the ASUPS formulation.

Let the finite element spaces which we wish to work with be given by

$$\mathbf{W}_h = \{\mathbf{w} \in H_0^1(\Omega)^N | V_k \in R_k(K)^N, K \in C_h\} \tag{14}$$

$$P_h = \{p \in C^0(\Omega) \cap L_0^2(\Omega) | p_k \in R_l(K), K \in C_h\} \tag{15}$$

where the integers k and l are greater than or equal to 1. Further let us consider a spectral/hp element discretization of Ω_f into subdomains, Ω_e, $k = 1, 2, ..., n_{el}$ where n_{el} is the number of spectral/hp elements into which the domain is divided. Based on this discretization, for the velocity and pressure, we define the trial discrete function spaces $\Im_u^{hp}$ and $\Im_p^{hp}$, and the weighting function spaces; $\mathbf{W}_u^{hp}$ and P_p^{hp} defined above. These spaces are selected, by taking the Dirichlet boundary conditions into account, as subspaces of $\left[H^{1h}(\Omega)\right]^{n_{el}}$ and $\left[H^{1h}(\Omega)\right]$, where $\left[H^{1h}(\Omega)\right]$ is the finite-dimensional function space over Ω_f. The first procedure of enforcing the velocity components enforces the velocity components directly on the nodes which are occupied by the solid domain with the aid of the extensional velocities from the solid to the fluid domain (18). We write the stabilized Galerkin formulation of eq. 12-13 as follows, find $\mathbf{u}^{hp} \in \Im_u^{hp}$ and $p^{hp} \in \Im_p^{hp}$ such that $\forall$

$\mathbf{w}^{hp} \in \mathbf{W}_u^{hp}$, $q^{hp} \in P_p^{hp}$

$$\int_{\Omega_f} \mathbf{w}^{hp}\rho \cdot \left(\frac{\partial \mathbf{u}^{hp}}{\partial t} + \mathbf{u}^{hp} \cdot \nabla \mathbf{u}^{hp} - \mathbf{f} \right) d\Omega_f - \int_{\Omega_f} \mathbf{w}^{hp} \cdot \nabla \cdot \sigma(p^{hp}, \mathbf{u}^{hp}) d\Omega_f +$$
$$\int_{\Omega_f} q^{hp} \nabla \cdot \mathbf{u}^{hp} d\Omega_f + \int_{\Omega_f} \epsilon q^{hp} p^{k,hp} d\Omega_f + \sum_{e=1}^{n_{el}} \int_{\Omega_f^e} \frac{1}{\rho} \tau \left(\rho \mathbf{u}^{hp} \cdot \nabla \mathbf{w}^{hp} + \nabla q^{hp} \right) \cdot$$
$$\left[\rho \frac{\partial \mathbf{u}^{hp}}{\partial t} + \rho \left(\mathbf{u}^{hp} \cdot \nabla \mathbf{u}^{hp} - f \right) - \nabla \cdot \sigma(p^{hp}, \mathbf{u}^{hp}) \right] d\Omega_f^e +$$
$$\sum_{e=1}^{n_{el}} \int_{\Omega_f^e} \delta \nabla \cdot \mathbf{w}^{hp} \rho \nabla \cdot \mathbf{u}^{\mathbf{hp}} d\Omega_f^e = \int_{\Gamma_h} \mathbf{w}^{hp} \cdot h^{hp} d\Gamma \tag{16}$$

As can be observed from Eqn. 16, four stabilizing terms are added to the standard Galerkin formulation. In Eqn. 16 the first three terms and the right hand side constitute the classical Galerkin formulation of the problem. The fourth term is an added stabilization term which results from the iterative regularization of the incompressibility equation. The surface integrals on the right are obtained from the weak form development as the natural boundary conditions. The first series of element-level integrals comprise the SUPG and PSPG stabilization terms, which are added to the variational formulation (7; 19). Prescriptions on determinations of the stabilization parameters based on inverse estimates have been utilized by Gervasio (20). In their paper the higher order stabilization parameter (with applications to spectral methods) was defined. A mathematical framework for obtaining the stabilization parameter not from ad-hoc estimates of the advective and diffusive limits but directly from stability analysis was provided in (12). The definition of the stabilization parameter is traditionally provided as

$$\tau(\mathbf{x}) = \frac{h_k}{2|u_h^n|_{pn} {N_d}^2} \xi(Re_k(\mathbf{x})) \tag{17}$$

where

$$Re_k(\mathbf{x}) = \frac{m|u_h^n|_{pn} h_k}{2\nu {N_d}^2} \tag{18}$$

$$\xi(Re_k(\mathbf{x})) = \begin{cases} Re_k(\mathbf{x})) \; Re_{k(\mathbf{x}))} \leq 1, \\ 1 \; 1 \leq Re_k(\mathbf{x})) \end{cases} \tag{19}$$

The next element level stabilization term on the continuity equation is the least squares incompressibility constraint (LSIC) term (21). This term is provided as

$$\delta_k = \frac{\lambda h_k |u_h^n|_{pn}}{{N_d}^2} \xi(Re_k(\mathbf{x})) \tag{20}$$

Obtaining a common bound on $\tau(Re_K(\mathbf{x}))$, with no restrictions on Re we arrive at

$$\tau(\mathbf{x}, Re_K(\mathbf{x})) \leq \frac{m_k h_k^2}{8\nu} \tag{21}$$

where

$$m_k = min\{\frac{1}{3}, 2C_k\} \tag{22}$$

In this paper we resort to the stabilization parameters defined by Eq. 17-20. In the above equations N_d denotes the number of degrees of freedom in each element. The constant m_k is defined above. The p norm of the velocity is defined

$$|\mathbf{u_h^n}(\mathbf{x})|_{pn} = \begin{cases} (|(u_h^n)_1(\mathbf{x})|^{pn} + |(u_h^n)_2(\mathbf{x})|^{pn})^{\frac{1}{pn}} \; 1 \leq pn \leq \infty, \\ max_{i=1,2}|(u_h^n)_i(\mathbf{x})| \; pn = \infty \end{cases} \tag{23}$$

We used the notation p to denote pressure and N to denote the space dimensions earlier. To avoid any confusion with notation we denote the p norm with pn and N_d as the number of degrees of freedom in each element. The above completes the ASUPS formulation for solving the FBM equations. The extensional velocity of the solid domain in this method is directly specified on the nodes occupied by the solid in Ω_i once the translational and angular velocity of each solid particle has been determined based on Eqn 4.

The second approach to the FBM specifies the velocity of the solid in a unified framework of both the solid and fluid as a continuum. The finite element formulation incorporating the solid domain velocity in the fluid equations is provided below. We write the stabilized formulation of eq. 1-2 considering the extensional velocity of the solid domain as a constraint in the functional as follows, Find $\mathbf{u}^{hp} \in \Im_u^{hp}$ and $p^{hp} \in \Im_p^{hp}$ such that $\forall\ \mathbf{w}^{hp} \in \mathbf{W}_u^{hp}$, $q^{hp} \in P_p^{hp}$

$$\begin{aligned} &\int_{\Omega_f} \mathbf{w}^{hp}\rho \cdot \left(\frac{\partial \mathbf{u}^{hp}}{\partial t} + \mathbf{u}^{hp} \cdot \nabla \mathbf{u}^{hp} - \mathbf{f}\right) d\Omega_f - \int_{\Omega_f} \mathbf{w}^{hp} \cdot \nabla \cdot \sigma(p^{hp}, \mathbf{u}^{hp}) d\Omega_f + \\ &\int_{\Omega_f} q^{hp} \nabla \cdot \mathbf{u}^{hp} d\Omega_f + \int_{\Omega_f} \epsilon q^{hp} p^{k,hp} d\Omega_f + \sum_{e=1}^{n_{el}} \int_{\Omega_f^e} \frac{1}{\rho}\tau \left(\rho \mathbf{u}^{hp} \cdot \nabla \mathbf{w}^{hp} + \nabla q^{hp}\right) \cdot \\ &\left[\rho \frac{\partial \mathbf{u}^{hp}}{\partial t} + \rho\left(\mathbf{u}^{hp} \cdot \nabla \mathbf{u}^{hp} - f\right) - \nabla \cdot \sigma(p^{hp}, \mathbf{u}^{hp})\right] d\Omega_f^e + \\ &\sum_{e=1}^{n_{el}} \int_{\Omega_f^e} \delta \nabla \cdot \mathbf{w}^{hp} \rho \nabla \cdot \mathbf{u^{hp}} d\Omega_f^e + \lambda \int_{\Omega_i} \mathbf{w} \cdot \left[(\mathbf{u} - \mathbf{u_i}) - \omega_i \times (\mathbf{X} - \mathbf{X}_i)\right]^2 d\Omega_i = \\ &\int_{\Gamma_h} \mathbf{w}^{hp} \cdot h^{hp} d\Gamma \end{aligned} \tag{24}$$

In this formulation the extensional velocity of the solid domain is viewed as a constraint and is included in a least squared sense into the ASUPS formulation. The specification of the penalty parameter λ is important for enforcing the correct velocity field on the solid domain. A sufficiently high value of the penalty parameter was found to provide satisfactory results. We confined the analysis to a constant value of $\lambda = 10^4$. Prescriptions on the determination of the iterative regularization constant have been provided in (12). The range of values of ϵ have been determined to be $[0, 0.03]$. We used the value of ϵ of 0.03.

4. Numerical Results

In this section we present numerical results obtained with higher order spectral/hp method with the FBM. We study flow past a circular shaped cylinder at Re-200. In later two dimensional examples we examine the flow past an ellipse shaped obstacle with different axis ratios and differing

boundary conditions. Finally we examine two ellipse shaped obstacles facing a free-stream, and two circular shaped obstacles. Anti-phase mode of vortex shedding is verified for the separation distance considered for the two circular shaped solid obstacles. As a three dimensional example we consider the flow past a ellipse shaped cylinder at a Reynolds number of 200.

4.1. *Unsteady Flow Past a Circular Cylinder*

We consider the unsteady flow past a circular cylinder at Reynolds number of 200. At this Reynolds number considered three dimensional effects are comparatively negligible. It has been observed that beyond Re-300 we obtain three dimensional wake with considerable interactions along the longitudinal direction of the cylinder. We consider the first FDM method for analysis for this two dimensional problem. A direct enforcement of the velocity components on the circular domain is required for the stationary cylinder with a velocity specification of $[u, v] = 0$. The center of the circular shaped obstacle is located at $[8, 8]$ inside a domain of size $[28, 16]$. The density of the fluid domain was taken as 1.0 with the viscosity of 0.005. The diameter of the cylinder was taken as 1.0 unit. The boundary conditions included a specification of the free stream velocity and no-penetration velocity at the left, bottom, and top faces of the computational domain. Pressure was specified to the datum value of $p = 0$ on the left face to anchor the pressure field. Traction free surface was specified as the exit plane.

The domain was partitioned into 40×40 elements with a p_{level} of 4 in each element. A minimum of 10 spectral elements were specified along the diameter of the cylinder. The problem was subject to unsteady analysis since at Reynolds numbers greater than Re-47 the problem exhibits unsteady behaviour. The time increment was taken as a constant value of $\Delta_t = 0.1$. The simulation was performed till a fully developed Von-Karman street had developed with a constant shedding frequency. Figure 1 presents the mesh used for the analysis along with the contour plot of the pressure at the instant of $t = 100$. The mesh refinement in the near vicinity of the cylinder ensures convergence of the approximate shape of the cylinder to a circular shape. Based on the problems solved it was found very accurate results could be obtained with 10 spectral elements along the diameter of the obstacle for all geometries studied.

The exit boundary conditions were specified to be non-reflecting and were found to not perturb the flow far upstream of the exit plane. The flow exits gracefully without any disturbances because of the exit plane boundary conditions. Figure 2 presents the unsteady contour plots of the u and v components of velocity at the non-dimensional time of $t = 100$. From the figure it is evident the shedding is fully developed. From the coefficient of lift for the problem we report a shedding frequency of 0.1754. The shedding period was found to be 5.7 time units. The time step taken for analysis provided 57 time steps through the shedding cycle. The shedding frequency was found to be close to the empirical relationship provided by Roshko (22) for flow past a circular cylinder as

$$St = 0.212 - \frac{4.5}{Re} \tag{25}$$

for Re-200 this equation provides an approximate Strouhal number of $St = 0.189$. The estimate from the equation is close to the value predicted by the simulation. The iterative regularization constant was taken as a value of 0.01 for this analysis. The velocity components of u and v were specified to have zero velocity to prescribe the cylinder.

4.2. *Unsteady Flow Past an Ellipse*

Flow past elliptical shaped cylinders is one of the important problems in CFD in the area of flow past bluff bodies. It is known that elliptical cylinders provide lesser resistance to the incoming flow and consequently have lower values of drag and lift. Unlike the canonical problem of flow past a circular shaped cylinder which has been studied extensively, data on flow past an ellipse shaped

cylinder is limited in literature. Let us define the axis ratio (AR) of the ellipse shaped cylinder as $AR = b/a$ where a and b are the semi-major axis and the semi-minor axis of the ellipse. The hydraulic diameter of the ellipse is defined as

$$d_h = \frac{4ab(64 - 16e^2)}{(a+b)(64 - 3e^4)} \quad e = \frac{a-b}{a+b} \tag{26}$$

For an axis ratio of 1.0 we recover a circle and for an axis ratio of 0.0 a flat plate.

It has been noted for circular shaped obstacles $AR = 1$ that vortex shedding is observed for $Re \geqslant 47$. In an earlier example we studied the shedding phenomenon for a Reynolds number of Re-200 for the axis ratio 1.0. As the circular shaped cylinder changes shape to an ellipse it has been observed there is a critical Reynolds number below which there is no observable occurrence of vortex shedding. The Reynolds number for which the vortex shedding is initiated is termed as the critical Reynolds number. When the axis ratio is reduced however as the circle turns into an oblong shape of an ellipse the shedding tends to be suppressed. The axis ratio above which there is shedding is termed as the critical axis ratio AR_{cr}. For a Reynolds number of $Re = 50$ the critical axis ratio has been found to be $AR = 0.9$ (23). The implication of the statement being if the axis ratio exceeds 0.90 and is close to 1.0 we expect to see the development of the Von-Karman vortex street. This is also in conformity with numerical simulations where it has been observed at Re$\geq$ 47 there is shedding of vortices for a circular cylinder. The critical ratio can be identified based on the time history of the lift coefficient.

For the flow problems considered in the problems following the Reynolds number is determined based on the hydraulic diameter of the ellipse d_h and the free-stream velocity u_∞. The problem was studied with two sets of boundary conditions. The first set of boundary conditions as prescribed by Raman et al. (23) required the specification of slip surfaces on the top and bottom face of the domain and a specification of the free-stream velocity $[1.0, 0]$ at the inlet to the computational domain. Pressure was specified at the left face as the datum pressure. Traction free exit surfaces completed the specification of the problem. The second set of boundary conditions considered the specification of free stream velocity at the inlet $(u, v) = [1, 0]$ at the top, and bottom boundaries. Pressure was specified at the inlet to the computational domain. The right exit face was assumed to be traction free. The differences observed in the results from both methods are provided in the paper.

Let us consider the flow past an elliptical shaped obstacle with the set of boundary conditions as prescribed by Raman (23). Two different axis ratios of 0.60 and 0.70 were considered. The simulations were performed till an end time of $t = 280$. The time increment considered was 0.10. Figure 3(a) presents the development of the u contour plot at the time instant of $t = 145$. The corresponding v component of the velocity is provided in Figure 3(b). It is evident that there is vortex shedding obtained for the axis ratio of $AR = 0.7$. Results for AR-0.6 are not being presented however they demonstrated flow separation behind the ellipse without any shedding phenomenon. The mass conservation of the FDM formulation for this Reynolds number was verified based on the ratio m_{out}/m_{in}. Figure 4 presents this ratio for the problem through the transient steps. There is excellent conservation of mass with the formulation and the errors in mass loss were found to lie between $0.01 - 0.15\%$. The lift coefficient of the ellipse for the Re-100 has been presented in Figure 5 for the hydraulic diameter of 1.0. The amplitude of the fluctuating lift was found to be 0.10 which was found to be very close to the reported values of 0.095 presented in Raman (23). This further verifies the predictive capabilities of the FBM method. In the figure we can verify the lift for the $AR = 0.60$ remains very low as there is no shedding involved.

To study the effects of the boundary conditions on this problem we impose a free-stream velocity on the top and bottom faces of the domain. Because of the free-stream velocity specifications the velocity component is bound to adhere to the no slip and no penetration conditions at these faces. Figure 6 presents the lift coefficient calculated for these boundary conditions. From the figure it is evident that the boundary condition lowers the critical axis ratio from 0.70 for the free slip

boundaries to $AR = 0.60$ for the free stream boundary specification. For lower values of the AR it is evident shedding was not perceptible and low values of lift were obtained. For an axis ratio of $AR = 0.4$ the lift history further corroborates no shedding is observed. The amplitude of the lift coefficient was found to be 0.06 for the free slip surface boundary condition for an axis ratio of AR=0.6.

4.3. *Unsteady Flow past Two Ellipses*

Experimental results of Williamson et al. (24) and others have considered flow past two cylinders and square shaped bodies at different Reynolds numbers and separation distances between the edges of the bodies $g*$. The gap between the two obstacles in the flowfield are denoted by $g*$ scaled by the diameter of the obstacle. Experimental observations based on inclusion of dye in the flow provided information on the dependence of the flow features with respect to the separation distance and Reynolds numbers. In the paper it was observed that either in-phase or anti-phase modes of shedding occur for long times for $g*$ in the range of 1.0-3.0 for circular cylinders. A special case of the separation distance $g*$ lying between 0.10-1.0 was examined since there is considerable interaction of both the wakes for this separation distance. The flow features for this configuration were mentioned as being relatively confused. The flow in such configurations becomes distinctly antisymmetric. For a very low separation distance of 0.3 it was realized that both bodies behave as a single body facing the free-stream. Flow experiments conducted clearly visualized the formation of a deflected gap flow even at low Reynolds numbers of Re-55 and the wake vortex pairs were found to have distinctly different sizes. To examine a similar problem however with ellipse shaped obstacles we consider the flow past two ellipses. This configuration is considered for various reasons, among them being the paucity of data for considerations of flow configurations past ellipse shaped obstacles.

The hydraulic diameter of the ellipses considered was $d_h = 1.1678$ with the semi major axis of 0.715 and semi-minor axis of 0.50. This provided an axis ratio of 0.70 for either ellipses. Reynolds number considered for the problem was Re-85. The Reynolds number was based on the free stream velocity of 1 and the hydraulic diameter of the ellipses. The computational domain was considered to have dimensions of $[28, 32]$. The center of both cylinders were placed at $[8, 15.075]$ and $[8, 16.925]$ respectively. The physical separation between the centers was thus 1.85. Scaled with the hydraulic diameter of the ellipse the separation distance was found to be $g* = 0.58$. The problem was considered for unsteady state analysis with a space-time decoupled formulation. The time increment was set at 0.1 time units. Figure 7 presents the u-contour plot for the two ellipse cylinders at the instant of time $t = 105$. The amalgamation of both the vortex streets are evident in this figure. There is extensive interaction of wakes from both cylinders for this separation distance between the cylinders. From the experimental observations of Williamson the mode of shedding lies in the 'anti-symmetric flow' region. The lower wake seems to dominate at this instant of time and the upper wake is relatively suppressed. The vortex pair have distinctly different sizes (24). The v-component of the velocity profiles have been provided in Figure 8. From the v-component of the velocities further it is evident the vortices interact extensively to form an amalgamated wake. Evolution of the pressure field is aided with an improved velocity-pressure coupling provided by the ASUPS formulation used for this simulation. The temporal evolutions of the pressure field are smooth in time. At the time instant of $t = 105$ the pressures have been presented in Figure 9.

The development of the lift on the top and bottom ellipses have been presented in Figure 10. For the flow past two ellipse shaped obstacles therefore we conclude the anti-phase mode of vortex shedding is dominant until around $t = 25$. At later times there is a gradual change of the flow field toward a single wake with nearly constant lifts experienced by the two cylinders.

4.4. *Unsteady Flow Past two Circular Cylinders*

To consider unsteady flow field in the presence of two circular cylinders we study the flow at a Reynolds number of Re=100. The Reynolds number was based on the free stream velocity, and the diameter of either cylinders facing the flow. The diameter of the cylinder was taken as $d = 1$. Experimental studies of such flows have been provided in Williamson et al. (24). They reported the flow is either in the anti-phase or in phase mode of shedding for long times for separation distances of $g*$ between $1.0 - 5.0$. It has been reported predominantly the anti-phase mode of shedding prevails from experimental observations giving rise to a vortex comprising of anti-phase parallel sheets. Although anti-phase mode of shedding has been reported it was further observed that it is possible for the flow to 'flip' suddenly to the inphase mode of shedding during experiments. In either case the flow behavior exhibits either inphase or anti-phase mode that prevail for long times.

We consider a two dimensional domain of dimensions $[32 \times 30]$ discretized into a 42×60 macro mesh. A p enrichment of 4 was considered in each element. Two cylinders of diameter 1.0 were placed at locations of $[8, 14.5]$ and $[8, 17.5]$ respectively. This provides a gap distance of $g* = 2.0$. A space-time decoupled formulation was considered for analysis. The time increment was taken at a constant value of 0.10. The problem was simulated till an end time of $t = 85$. Anti-phase mode of shedding was found to be dominant for this flow configuration for the whole time of the simulation. Figure 11 presents the u and v contours of the flow field for the problem. Both the cylinders were found to experience approximately the same drag. The mean value of the drag was found to be 2.03 and 1.97 respectively. The fluctuating component of the lift coefficient with time for the lower cylinder has been presented in Figure 12. The amplitude of the lift was found to be approximately 0.54. Two probe locations were identified at horizontal separation of 2.0 units from the center of the cylinders. The locations of the probes were determined as $[10, 14.5]$ and $[10, 17.5]$ respectively. The history plots for the v-component of the velocities are presented in Figure 13. Anti-phase mode of shedding is clearly verified.

4.5. *Flow past a Three Dimensional Ellipse*

Let us consider studying flow past a fully immersed ellipse in $3D$ with Fictitious Boundary Methods. We consider a computational domain of dimensions $[14 \times 12 \times 2]$. The height of the three dimensional ellipse was considered to be h=2 units from the bottom face of the domain. Reynolds number considered for analysis was taken as Re-200. Accordingly, the viscosity of the fluid was taken as $\nu = 0.0025$. The semi-major and semi-minor axis were considered to be of length $a = 0.611878$ and $b = 0.428315$ respectively. Reynolds number was based on the hydraulic diameter of the ellipse and the velocity of free stream of $u = 1$. Inlet to the computational domain was considered on the left face of the domain. The center of the ellipse was placed at the location of $[5, 6, 0]$ with a domain height of 2 units. This places the ellipse symmetrically at the center from the walls of the computational domain.

On the boundaries of the immersed cylinder in the free stream Γ_h we prescribe values of the velocity components $(u, v, w) = (0, 0, 0)$. A free stream velocity of $\mathbf{u} = (1, 0, 0)$ was specified on the inlet, front, and back face boundaries. No-penetration boundary condition was specified at the bottom, top, front, back, and left faces. The exit was assumed to be traction free $t_y = 0$. No velocity component in the third dimension was specified at all faces other than the exit face which was assumed to be traction free with $t_z = 0$. The exit face was specified to be traction free in all three components of $t_x = t_y = t_z = 0$. Pressure was specified as the datum pressure at the inlet to the computational domain of $p = 0$ at the left face. Fluctuations on the lift coefficient and the x-component of the drag force on the elliptical cylinder were the metrics of interest.

We determine the coefficients with the help of integration of the forces on the sides of the cylinder. Let us denote the direction cosines of the inward normal with $(n_y, -n_x, n_z)$. Let S denote the surface of the cylinder. The drag, lift and tangential forces were calculated with the above

formulae

$$\mathbf{F} = \int_S \sigma \cdot \mathbf{n} d\mathbf{S} \tag{27}$$

The stress tensor is evaluated for Newtonian fluids as

$$\sigma = -p\mathbf{I} + 2\mu \left(\nabla \mathbf{u} + \nabla \mathbf{u}^T \right) \tag{28}$$

The force coefficients were evaluated with the above formulae

$$\begin{aligned} c_d &= \frac{2F_d}{\rho \bar{U}^2 D} \\ c_l &= \frac{2F_l}{\rho \bar{U}^2 D} \\ c_z &= \frac{2F_z}{\rho \bar{U}^2 D} \end{aligned} \tag{29}$$

We subject the three-dimensional problem for transient analysis. The domain was meshed into a macro mesh comprising of $28 \times 28 \times 4$ elements. A p enrichment of 4 in each element was considered for the space-time decoupled analysis. Ten elements were used in the band of cells which described the geometry of the ellipse in the flow. The problem was simulated till an end time of 50 units with a time increment specified to 0.10. Figure 14 presents the iso-contour plot of the v-velocity at the Reynolds number of Re-200 at the instant of time $t = 48.0$. The corresponding w-velocity component for the ellipse problem is presented in Figure 15. As can be seen from the figure there is considerable development of the third component w of the velocity for this problem. The considerable velocity interactions with the ellipse shaped obstacle allowed a higher aspect ratio ($AR = 0.70$) for this geometry to not obtain a shedding phenomenon for the time of simulation. The mean drag coefficient for the partially immersed cylinder was found to be 1.0. The mean value of the lift coefficient was found to be zero for the problem as observed from Figure 16.

5. Conclusion

In this paper we present the integration of the Augmented SUPS formulation (ASUPS) with Fictitious Boundary Method (FBM). Two different formulations for solving the FBM problem are described. Fixed Cartesian product grids are utilized to solve flow past different shaped obstacles. We utilize the FBM method to obtain benchmark results for the drag and lift for circle, and ellipse shaped obstacles. Further on the method is extended to solve flow past two ellipse and circle shaped obstacles. Anti-phase mode of shedding is verified for both problems. We examine the flow past a three dimensional ellipse as an example in three dimensional computations. Faithful metrics of all fields of interest are resolved on relatively coarse macro meshes by utilizing spectral elements for the problems of interest. With the procedures described we implement simplified Cartesian product grids for solving solid-fluid flow interaction problems.

References

[1] D. Wan and S. Turek, "Fictitious boundary and moving mesh methods for the numerical simulation of rigid particulate flows," *Journal of Computational Physics*, vol. 222, no. 1, pp. 28–56, 2007.

[2] J. Reddy, "On penalty function methods in the finite-element analysis of flow problems," *International Journal for Numerical Methods in Fluids*, vol. 2, no. 2, pp. 151–171, 1982.

[3] B. Jiang, *The least-squares finite element method: theory and applications in computational fluid dynamics and electromagnetics*. Springer, 1998.
[4] R. Ranjan, *hp-spectral methods for structural mechanics and fluid dynamics problems*. Texas A&M University, 2010.
[5] R. Ranjan and J. Reddy, "On multigrid methods for the solution of least-squares finite element models for viscous flows," *International Journal of Computational Fluid Dynamics*, vol. 26, no. 1, pp. 45–65, 2012.
[6] A. Brooks and T. J. Hughes, "Streamline upwind/petrov-galerkin methods for advection dominated flows," in *Third Internat. Conf. of Finite Element Methods in Fluid Flow, Banff, Canada*, 1980.
[7] A. N. Brooks and T. J. Hughes, "Streamline upwind/petrov-galerkin formulations for convection dominated flows with particular emphasis on the incompressible navier-stokes equations," *Computer methods in applied mechanics and engineering*, vol. 32, no. 1, pp. 199–259, 1982.
[8] T. J. Hughes and A. Brooks, "A theoretical framework for petrov-galerkin methods with discontinuous weighting functions: Application to the streamline-upwind procedure," *Finite elements in fluids*, vol. 4, pp. 47–65, 1982.
[9] J. Reddy and D. Gartling, *The finite element method in heat transfer and fluid dynamics*. CRC Press, 2010.
[10] T. J. Hughes and A. Brooks, "A multidimensional upwind scheme with no crosswind diffusion," *Finite element methods for convection dominated flows, AMD*, vol. 34, pp. 19–35, 1979.
[11] Y. Bazilevs, K. Takizawa, and T. E. Tezduyar, *Computational fluid-structure interaction: methods and applications*. John Wiley & Sons, 2013.
[12] R. Ranjan, Y. Feng, and A. T. Chronopolous, "Augmented stabilized and galerkin least squares formulations," *Journal of Mathematics Research*, vol. 8, no. 6, pp. 1–33, 2016.
[13] R. Ranjan and J. Reddy, "hp-spectral finite element analysis of shear deformable beams and plates," *Journal of Solid Mechanics*, vol. 1, no. 3, pp. 245–259, 2009.
[14] R. Ranjan, "Nonlinear finite element analysis of bending of straight beams using hp-spectral approximations," *Journal of Solid Mechanics*, vol. 3, no. 1, pp. 96–113, 2011.
[15] R. Ranjan, A. T. Chronopoulos, and Y. Feng, "Computational algorithms for solving spectral/hp stabilized incompressible flow problems," *Journal of Mathematics Research*, vol. 8, no. 4, p. 21, 2016.
[16] R. Ranjan, Y. Feng, and A. Chronopoulos, "Procedures for solving spectral/hp stabilized incompressible flow problems," *University of Texas, San Antonio, Department of Computer Science, Technical Report*, 2016.
[17] R. Ranjan and J. Reddy, "Non uniform rational bspline (nurbs) based non-linear analysis of straight beams with mixed formulations," *Journal of Solid Mechanics*, vol. 8, no. 4, pp. 1–12, 2016.
[18] S. Turek, D. Wan, and L. S. Rivkind, *The Fictitious Boundary Method for the implicit treatment of Dirichlet boundary conditions with applications to incompressible flow simulations*. Springer, 2003.
[19] T. J. Hughes, L. P. Franca, and M. Balestra, "A new finite element formulation for computational fluid dynamics: V. circumventing the babuška-brezzi condition: A stable petrov-galerkin formulation of the stokes problem accommodating equal-order interpolations," *Computer Methods in Applied Mechanics and Engineering*, vol. 59, no. 1, pp. 85–99, 1986.
[20] P. Gervasio and F. Saleri, "Stabilized spectral element approximation for the navier–stokes equations," *Numerical Methods for Partial Differential Equations*, vol. 14, no. 1, pp. 115–141, 1998.
[21] T. Tezduyar and S. Sathe, "Stabilization parameters in supg and pspg formulations," *Journal of computational and applied mechanics*, vol. 4, no. 1, pp. 71–88, 2003.
[22] A. Roshko, "Experiments on the flow past a circular cylinder at very high reynolds number," *Journal of Fluid Mechanics*, vol. 10, no. 03, pp. 345–356, 1961.
[23] S. K. Raman, K. A. Prakash, and S. Vengadesan, "Effect of axis ratio on fluid flow around an elliptic cylinder using immersed boundary method," in *Proceedings of Thirty Seventh National and Fourth International Conference on Fluid Mechanics and Fluid Power. Indian Institute of Technology Madras, Chennai*, 2010.
[24] C. Williamson, "Evolution of a single wake behind a pair of bluff bodies," *Journal of Fluid Mechanics*, vol. 159, pp. 1–18, 1985.

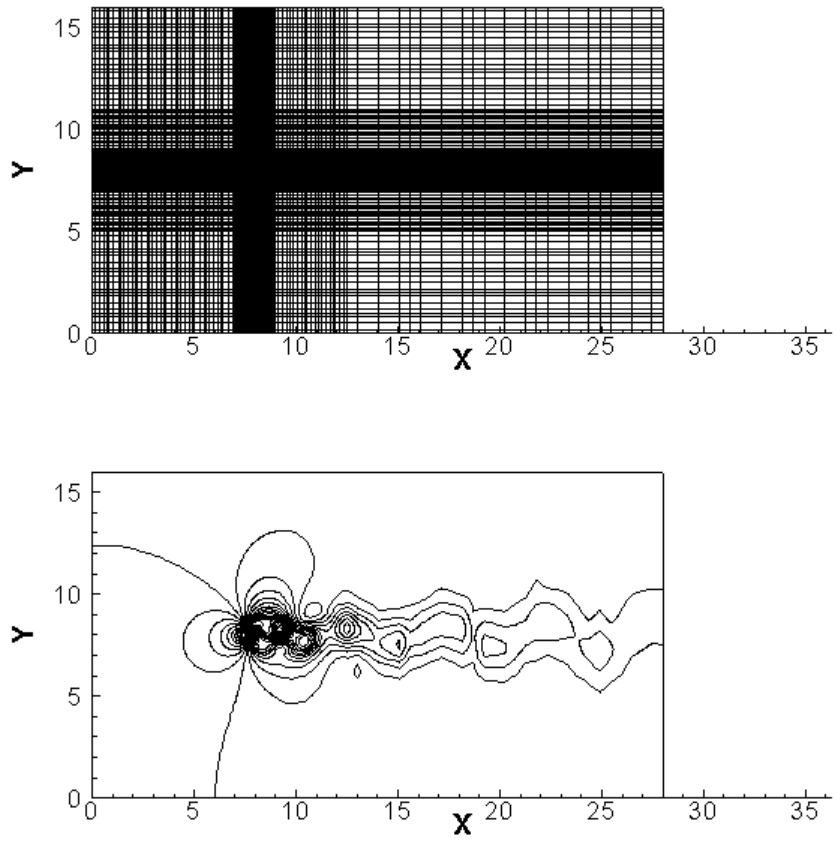

Figure 1. Re-200 Mesh and pressure contour plot (t-100)

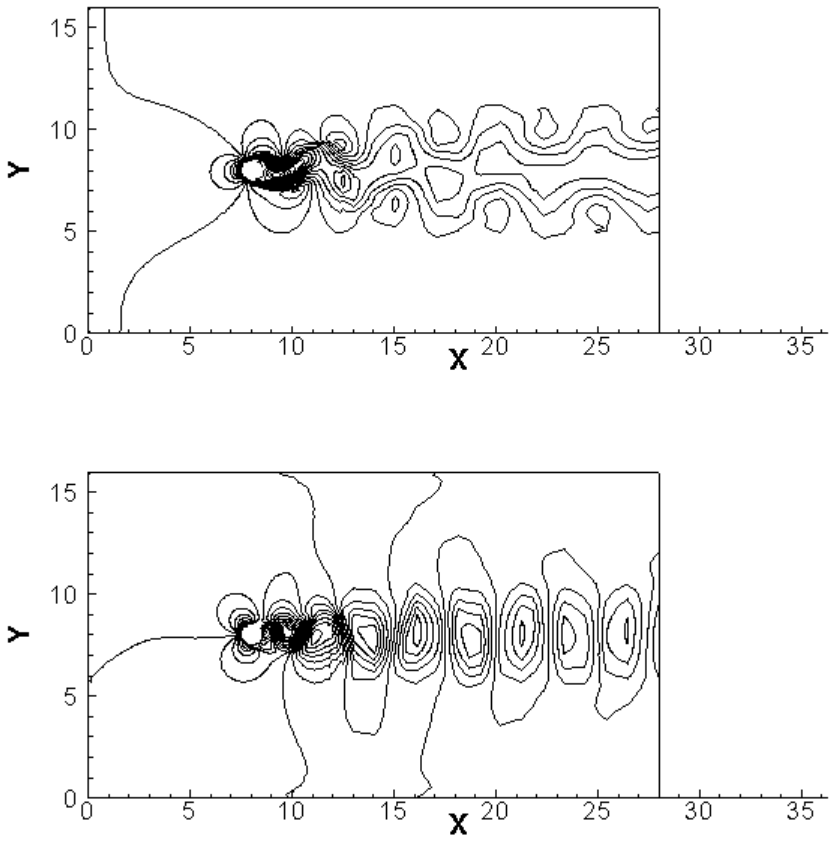

Figure 2. Re-200 U,V Contour Plots (t-100)

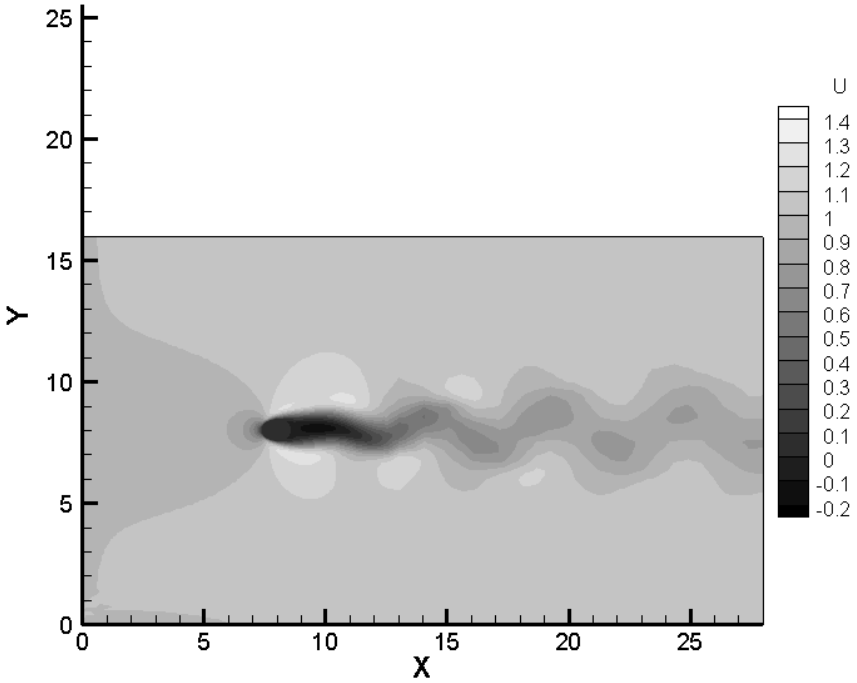

(a) U Contour

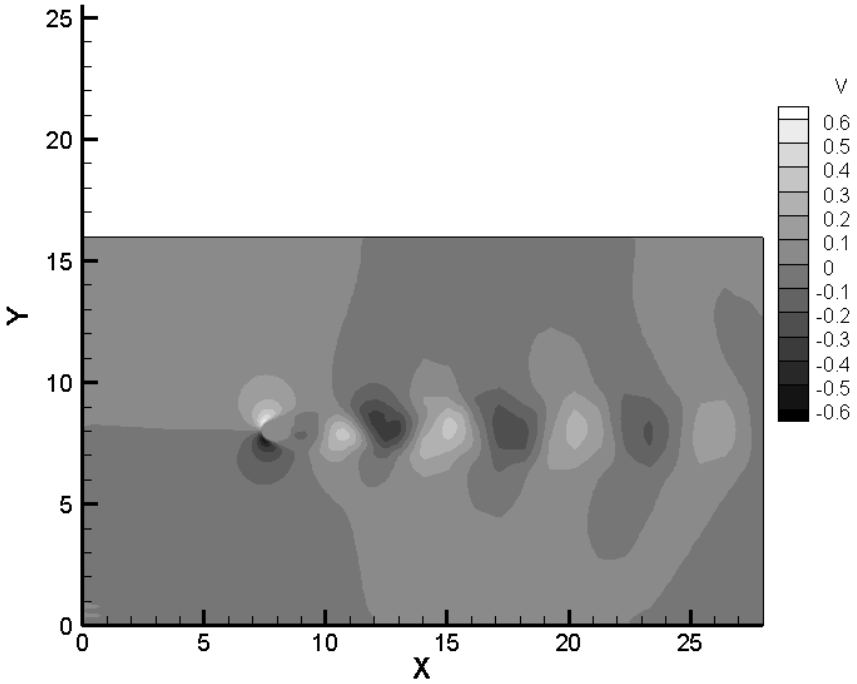

(b) V Contour

Figure 3. Flow past ellipse AR 0.70 U and V contour (t-145)

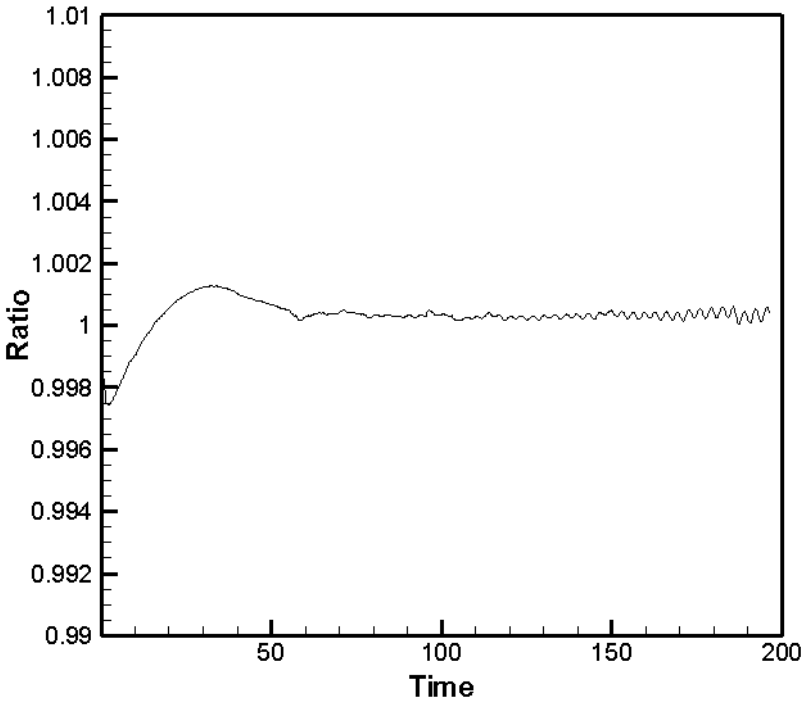

Figure 4. Mass Conservation at exit plane for Ellipse

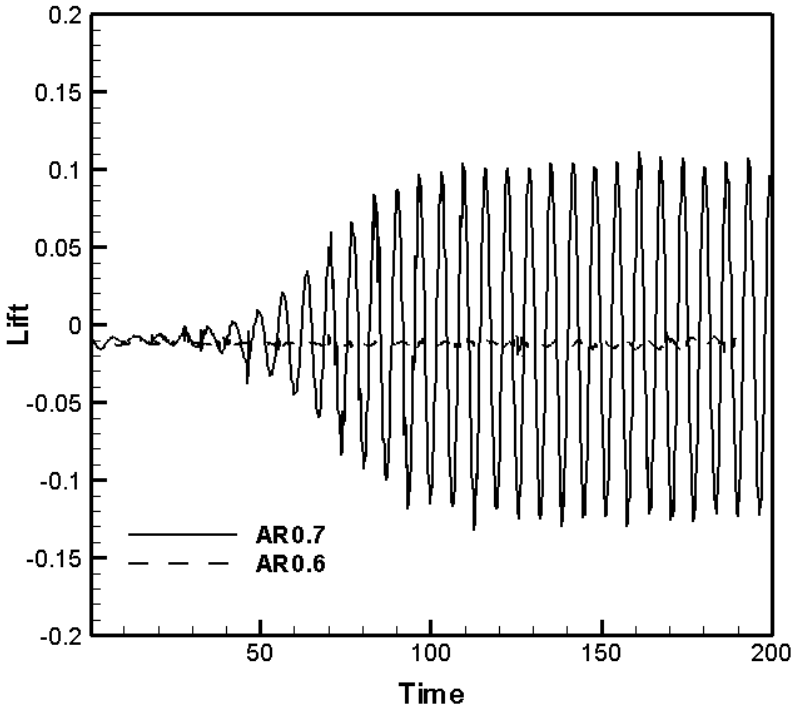

Figure 5. Lift Coefficient for ellipse (hydraulic diameter 1.0)

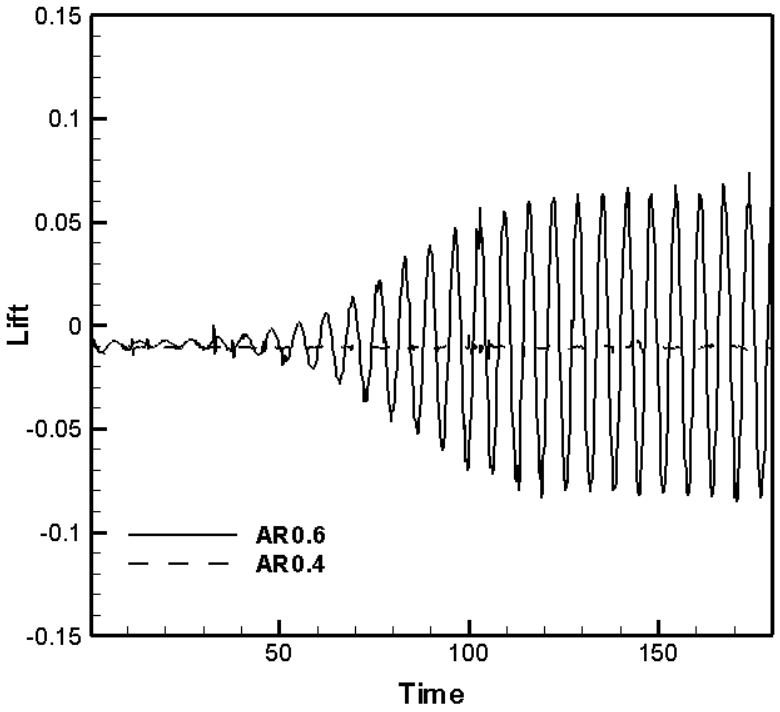

Figure 6. Lift Coefficient for ellipse in free stream

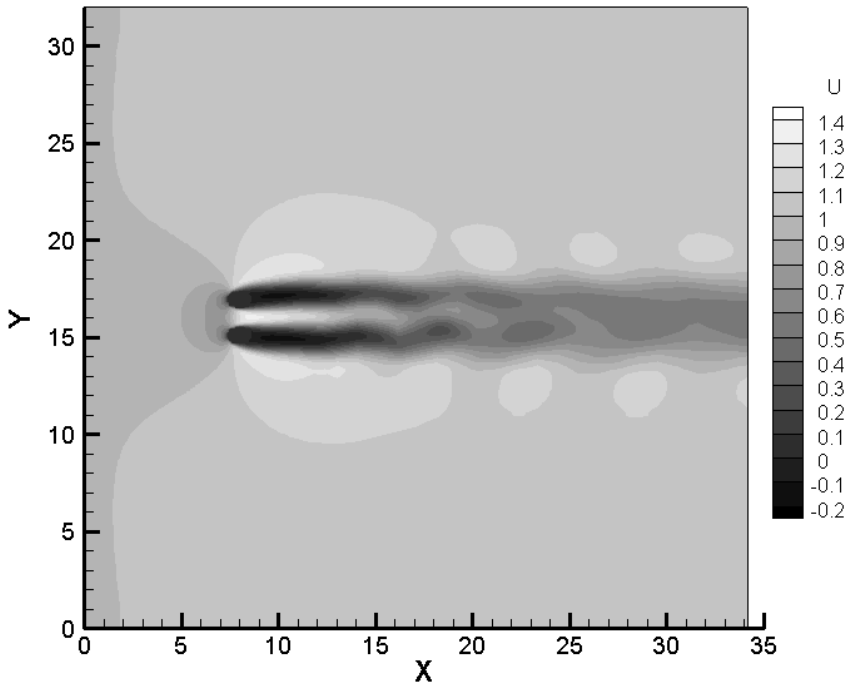

Figure 7. Contour plot of U velocity component (t-105)

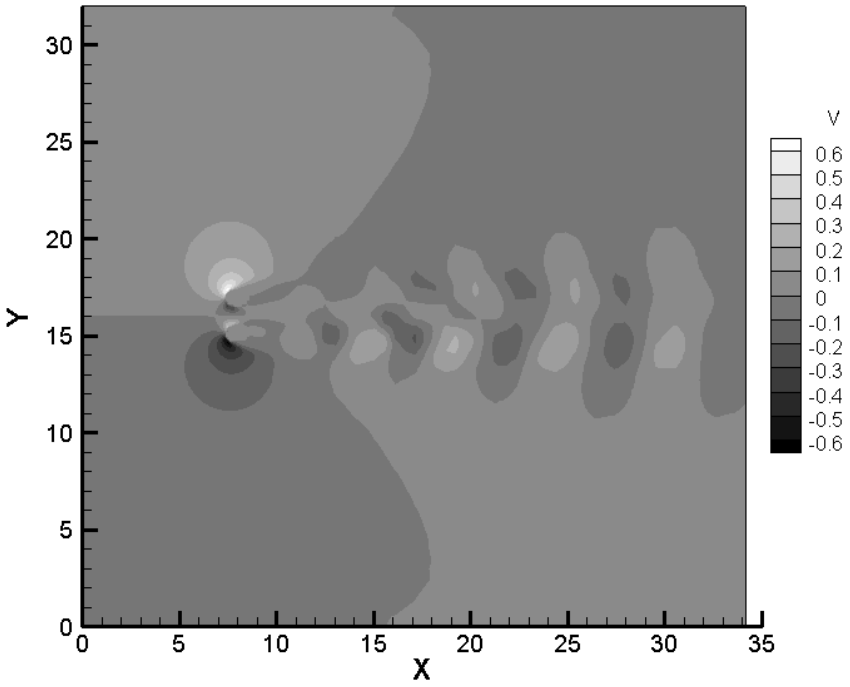

Figure 8. Contour plot of V velocity component (t-105)

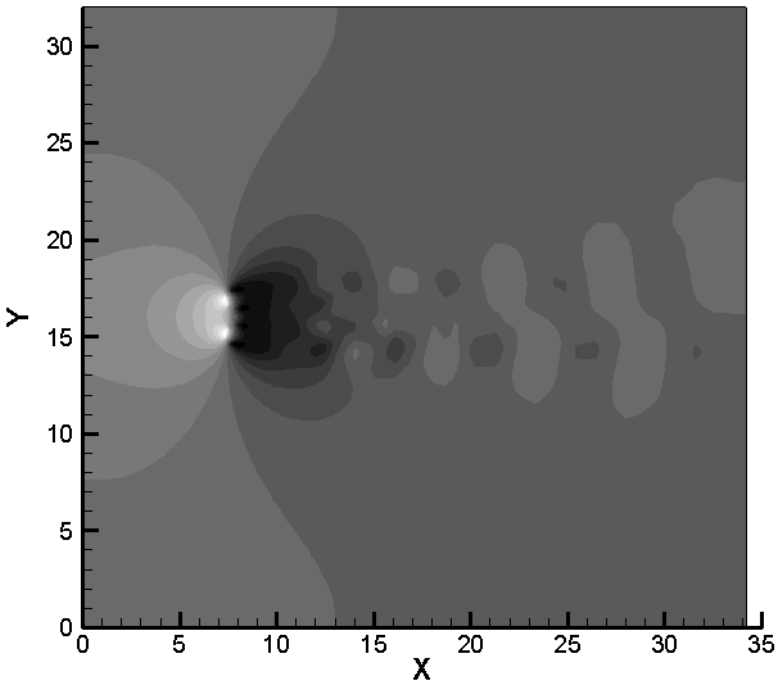

Figure 9. Pressure Contours (t-105)

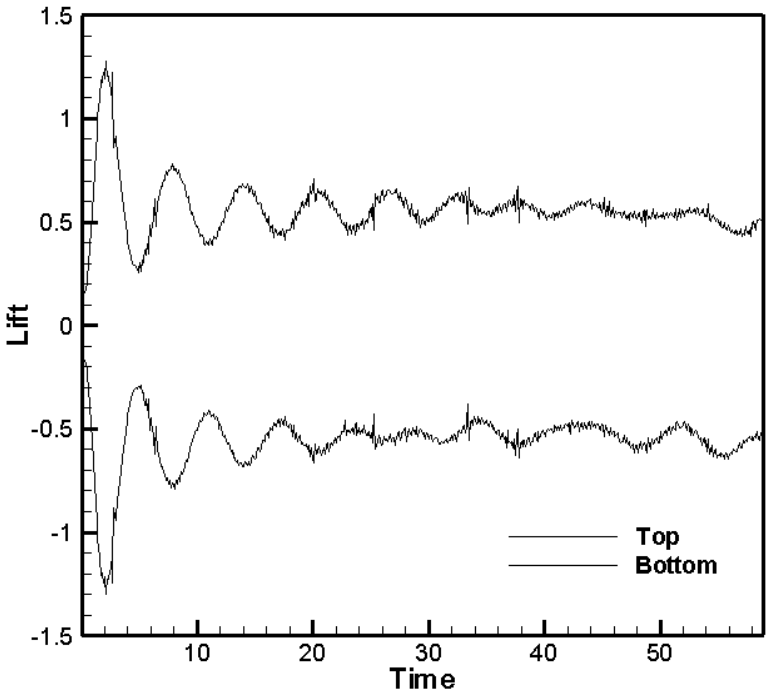

Figure 10. Lift Coefficient for two ellipses in flow field

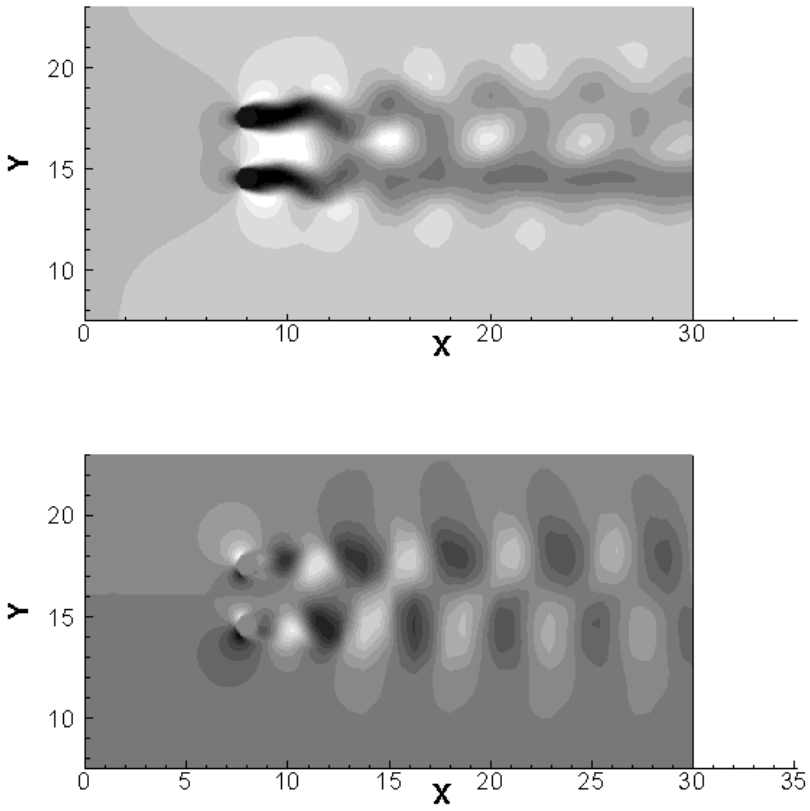

Figure 11. u-velocity and v-velocity contour plots S/D=2

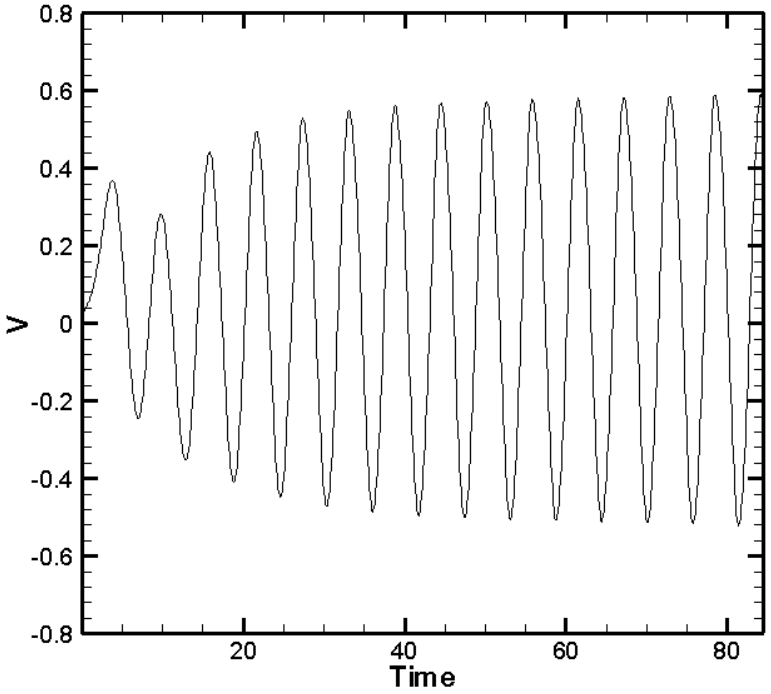

Figure 12. Lift Coefficient for Bottom Cylinder in FlowField

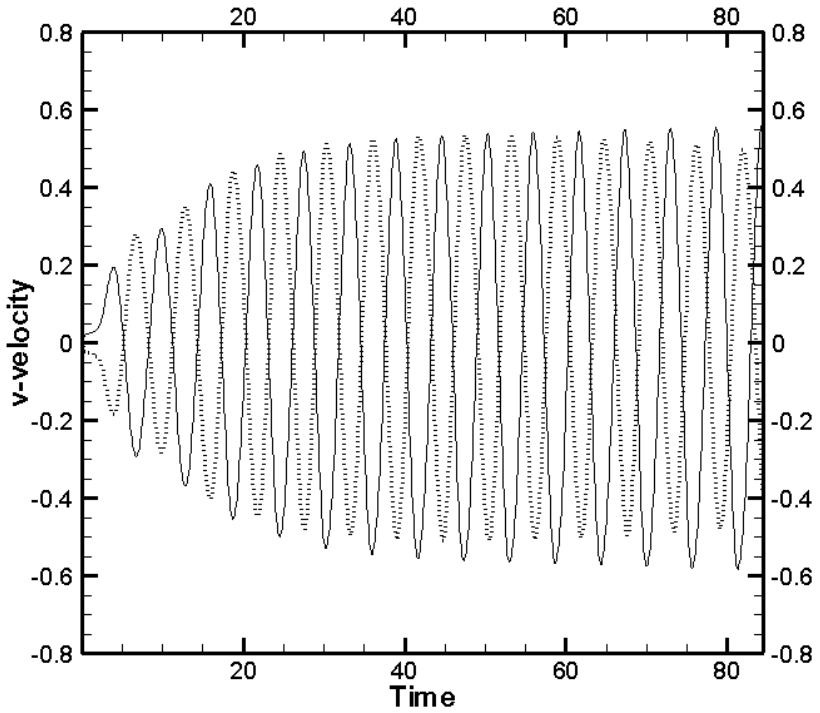

Figure 13. v-velocity at locations [10,14.5] and [10,17.5]

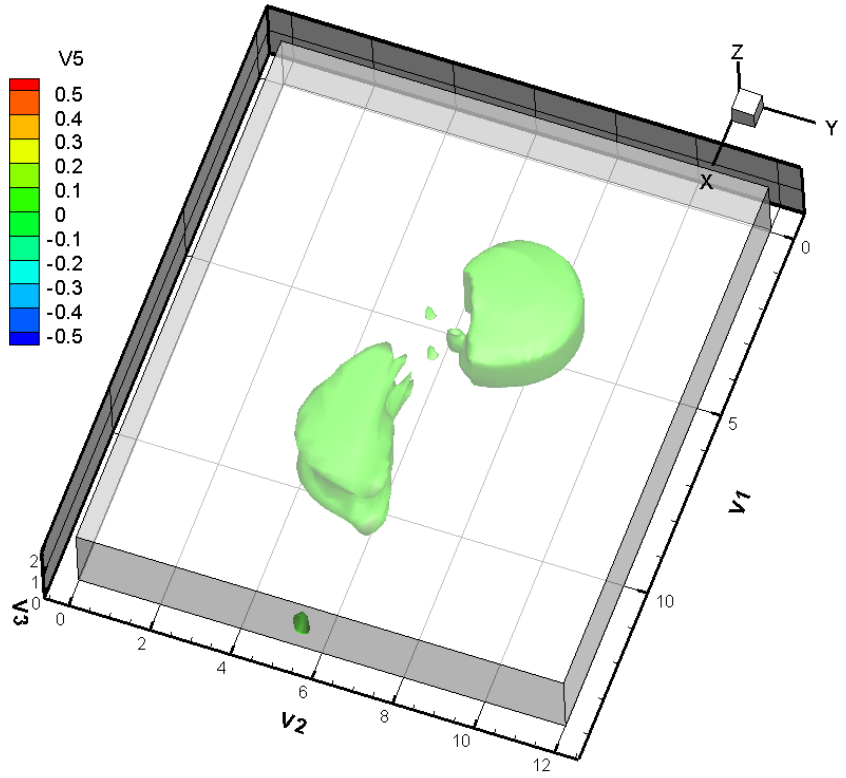

Figure 14. V component isocontours Re-200

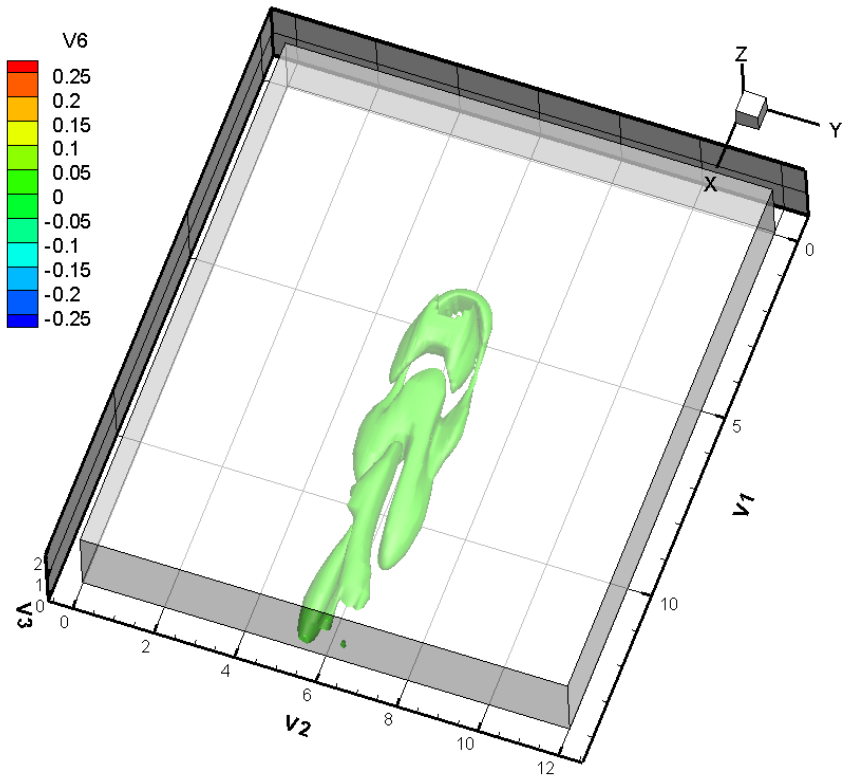

Figure 15. W component isocontours Re-200

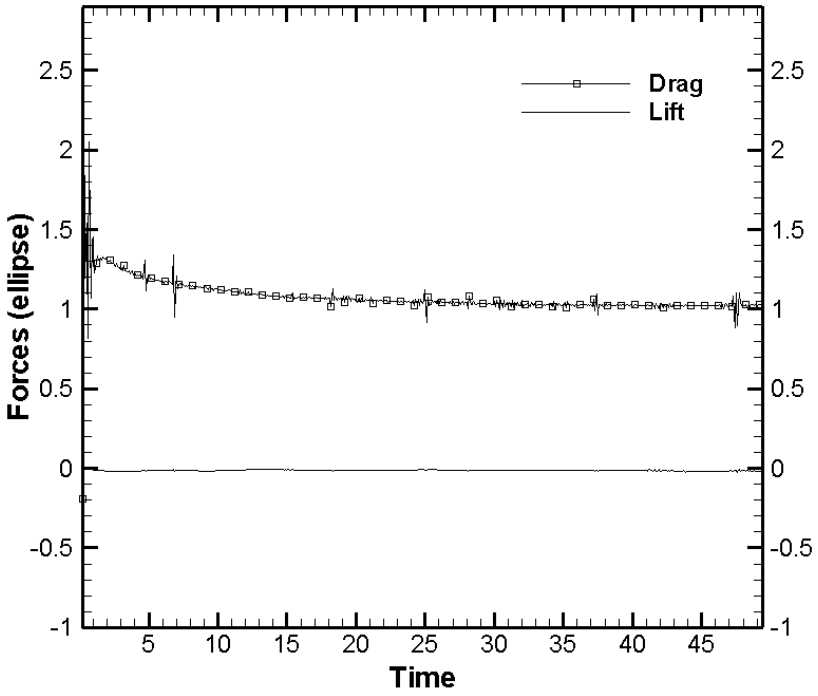

Figure 16. Drag and lift flow past an ellipse in 3D